2024 IEEE/RSJ International Conference on Intelligent Robots and Systems (IROS)
October 14-18, 2024. Abu Dhabi, UAE

Development of a Spherical Wheel-legged Composite Mobile Robot with Multimodal Motion Capabilities

Yuyang Du, Ruihua Ye, and Wenfu Xu*, *Senior Member, IEEE*

***Abstract*—In this paper, we present a spherical wheel-legged mobile robot, aiming to meet the demands of adaptability to complex terrains and high maneuverability. It consists of a spherical main body and five-bar linkage parallel wheel-legged mechanisms. It can switch between legged and spherical modes by extending and retracting its legs according to the demands of the actual environment, thereby enhancing the overall mobility of the robot. By designing the Linear Quadratic Regulator (LQR) controller, we achieve the impact-resistant leg balancing motion and autonomous pitch adjustment for the robot on inclined surfaces in the legged configuration. For the rolling control in the spherical configuration, a hierarchical sliding mode control method and Proportional-Integral-Derivative controller (PID) are employed to control the rolling and turning of the robot. We verify the robustness of the robot in wheel-legged configuration against disturbances and the stability of its motion in spherical configuration.**

I. INTRODUCTION

Currently, most mobile robots have limited motion modes, making it difficult to balance performance requirements such as adaptability to the environment, obstacle avoidance capability, speed and efficiency. Therefore, this paper proposes a design for a spherical leg-wheel composite mobile robot with multiple configurations. It can switch between different motion modes based on the environment, thereby enhancing the overall performance of the robot.

Various driving methods and control approaches have been proposed by researchers internationally for spherical robots, including single-pendulum and double-pendulum drives (e.g., [1-4]). To address the weak obstacle avoidance capability of spherical robots, the development of hybrid spherical robots has become an important research direction. For example, KisBot [5] and BYQ-XI [6] enhance terrain traversability by employing auxiliary linkages to support the spherical robot. SphereX [7] and RolLeapO [8] use two hemispherical shells as wheels and install a catapult mechanism at the bottom of the robot, enabling jumping and improving obstacle crossing ability. QroSS [9] has achieved spherical rolling and legged crawling, enhancing the robot's terrain adaptability. Bipedal wheeled-leg robots combine the characteristics of wheels and legs, providing flexible mobility and strong terrain adaptability. For example, the WLR series [10],[11] exhibit robust stability and obstacle traversal capability. They have larger dimensions and weight, utilizing hydraulic actuation for high power density. Ascento [12] and Olie [13] are primarily designed for indoor exploration and navigation, offering greater flexibility and cooperation. However, there is currently no research that combines the advantages of spherical and wheeled-leg robots. By integrating their strengths, it has the potential to enhance the overall mobility of robots.The robot can move at high speed on flat ground or inclined plane without fear of overturning in spherical form, and the spherical shell can also make it carry out tasks in special environments such as pipelines, and at the same time, due to the small rolling friction consumption, it has obvious advantages in energy utilization efficiency; The wheel-legged form can cross ravines and steps of a certain height, which is not possible with spherical robots.

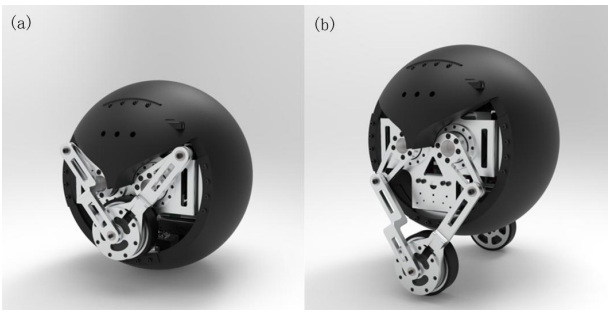

Fig. 1: Rendered image of the spherical wheel-legged robot. (a)In the spherical configuration . (b) In the wheel-legged configuration.

This paper focuses on the following achievements: (1) Designing a spherical wheel-legged mobile robot ,shown in Figure 1, which combines the capabilities of spherical rolling and legged locomotion to enhance its overall mobility. (2) Achieving multimodal dynamic modeling of the robot, including legged balancing and spherical rolling.(3) Utilizing LQR, hierarchical sliding mode, and PID controllers to achieve multimodal motion in the robot. Section II introduces the hardware platform of the robot. Section III completes the dynamic modeling of the robot based on the structural parameters. Section IV describes the control architecture and hardware experimental results presented in Section V. Finally, Section VI provides the conclusion.

* This work was supported in part by the National Natural Science Foundation of China (Grant No. 62233001), Program of Shenzhen Peacock Innovation Team (Grant No. KQTD20210811090146075), and the Basic Research Program of Shenzhen (JCYJ20220818102415034). (Corresponding Author: Wenfu Xu).

The authors are with the School of Mechanical Engineering and Automation, Harbin Institute of Technology, Shenzhen 518055, China. They are also with Guangdong Key Laboratory of Intelligent Morphing Mechanisms and Adaptive Robotics, Shenzhen 518055, China.

II. DESIGN

A. Overview

The overall framework and internal module arrangement of the spherical-wheeled legged mobile robot are shown in Figure 2. It mainly consists of a spherical shell, base side plates, brackets, motion joint modules , servos, and other sensors. The robot uses a spherical shell as its body and in the spherical rolling mode, it generates driving torque through internal mass offset. A two-degree-of-freedom pendulum mechanism is employed to drive the rolling motion of the

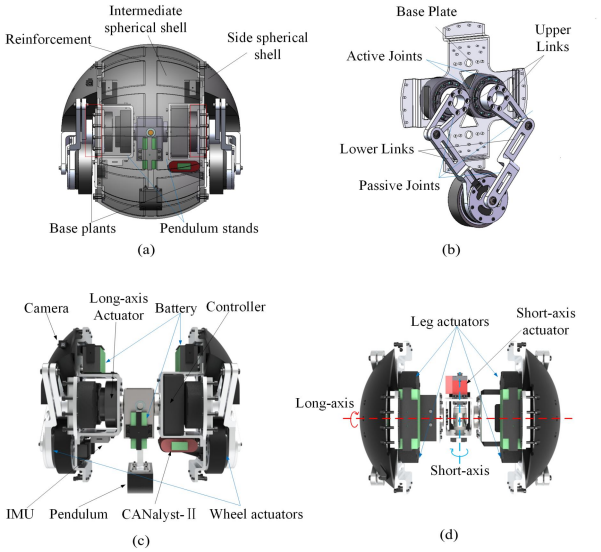

Fig. 2: Robot structure. (a) Robot main mechanical framework. (b) Five-bar parallel wheel-leg structure (c) Front view (with hidden sphere shell). (d) top view (with hidden sphere shell)

sphere. The pendulum can swing around mutually orthogonal long and short axes, enabling the robot to perform longitudinal and lateral rotations in the spherical rolling mode. Each of the swings around the long and short axes is driven by a joint module.

B. Leg Design

To achieve rapid and reliable shape shifting, the legs are arranged on either side of the sphere. The leg structure of the robot is shown in Figure 2(b). The legs adopt a five-bar parallel structure, driven by two joint modules. This structure has higher stiffness, stronger load-bearing capacity, and greater explosive force compared to a series structure. Due to the spherical body, its size is much larger than the wheels at the feet, giving the sphere a greater advantage in terms of rolling speed and obstacle-crossing ability compared to the wheels at the feet. In the wheel-leg configuration, the legs extend, lifting the sphere off the ground, while the two wheels make contact with the ground. Internal pendulum movements can also be performed to achieve the desired motion state in coordination with the robot.

C. Computing and Control Architecture

The robot has multi-threaded computing capabilities and can respond in real-time based on the collected information. The main controller selected is the Intel NUC11TNKi7, which can provide powerful computational capabilities and offering a variety of USB interfaces. The Inertial Measurement Unit (IMU) is applied to collect the rotational velocities and linear accelerations in three axes. It utilizes the Kalman fusion algorithm to calculate attitude information and provide quaternion representation of the attitude. The sensor has a maximum output frequency of 400Hz, meeting real-time requirements, with pitch and roll angle errors within 0.1° and yaw angle error within 0.5°.Additionally, this sensor supports the Robot Operating System (ROS) platform and can be directly used via the USB interface. All joint motors are capable of receiving commands sent from the upper computer and providing feedback on the current joint information.

III. DYNAMIC MODELING

A. Dynamic Modeling of Wheel-leg Balance Control

To consider the mutual influence between the pendulum and the leg-wheel system, we treat the robot's body and legs as an inverted pendulum. The simplified structure of the robot is shown in Figure 4.

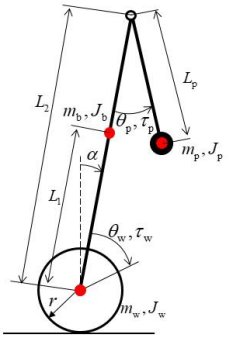

Fig. 4: Inverted pendulum with a wheeled cart model

In the diagram, $\alpha, \theta_w, \theta_p$ represent the robot's pitch angle, the wheel's angle relative to the inverted pendulum, and the pendulum's angle relative to the inverted pendulum. τ_w, τ_p are the torques applied to the wheel and pendulum joints.. m_w, m_b, m_p are the masses of a single wheel, the inverted pendulum and the pendulum.

By selecting $\boldsymbol{q} = [\alpha \quad \theta_w \quad \theta_p]^T$ as the generalized coordinates, the generalized velocity is $\dot{\boldsymbol{q}} = \left[\dot{\alpha} \quad \dot{\theta}_w \quad \dot{\theta}_p\right]^T$. Let the kinetic energy of the two wheels be T_1, the kinetic energy of the inverted pendulum be T_2 and he kinetic energy of the pendulum be T_3.The total kinetic energy of the system can be expressed as:

$$T_{\text{sys}} = T_1 + T_2 + T_3 \tag{1}$$

Assuming the potential energy of the wheels is zero, let the potential energy of the inverted pendulum be V_2 and potential

energy of the heavy pendulum be V_3.The total potential energy of the system can be expressed as V_{sys}:

$$V_{\text{sys}} = V_2 + V_3 \tag{2}$$

Defining the Lagrangian function $L = T_{\text{sys}} - V_{\text{sys}}$, then we can get :

$$\frac{d}{dt}\left(\frac{\partial L}{\partial \dot{\boldsymbol{q}}_i}\right) - \frac{\partial L}{\partial \boldsymbol{q}_i} = \sum_{k=1}^{3} \boldsymbol{M}_k \frac{\partial \boldsymbol{\omega}_k}{\partial \dot{\boldsymbol{q}}_i} \tag{3}$$

where $\boldsymbol{\omega}_k$ represents the rotational velocity of rigid body k, and $\boldsymbol{M}_k$ represents the torque applied to rigid body k.

The dynamic equations of the system can be expressed as:

$$\boldsymbol{M}(\boldsymbol{q})\ddot{\boldsymbol{q}} + \boldsymbol{V}(\boldsymbol{q}, \dot{\boldsymbol{q}}) = \boldsymbol{B}^T \boldsymbol{u} \tag{4}$$

Where $\boldsymbol{M} \in \mathbb{R}^{3\times3}$ represents the inertia matrix , $\boldsymbol{V} \in \mathbb{R}^{3\times1}$ represents the nonlinear terms, $\boldsymbol{B} \in \mathbb{R}^{2\times3}$ is the torque mapping matrix, and $\boldsymbol{u}$ is the joint torque vector, $\boldsymbol{u} = [\tau_w \quad \tau_p]^T$.

B. Dynamic Modeling of Spherical Rolling

The longitudinal rolling subsystem and lateral swinging subsystem are shown in Figure 5, from the perspectives of the y-axis and x-axis of the heading coordinate system {G}. In the diagram, $\alpha, \beta, \theta_{\text{p1}}, \theta_{\text{p2}}$ represent the robot's pitch angle, roll angle, long-axis joint angle of the pendulum, and short-axis joint angle of the pendulum, respectively. $L_{\text{p1}}, L_{\text{p2}}$ are the effective pendulum lengths in the longitudinal subsystem and lateral subsystem. They represent the projection lengths of the actual pendulum length L_p onto the XOZ and YOZ planes of the {G} coordinate system.

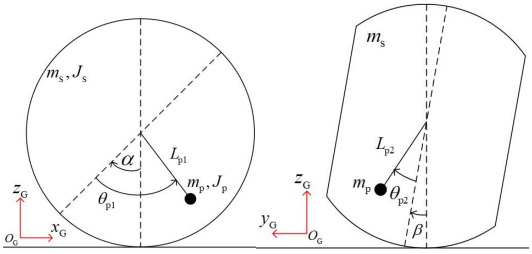

(a) (b)

Fig. 5: Rolling subsystem. (a) The longitudinal rolling subsystem. (b)The lateral swinging subsystem.

Using the Lagrangian method, let the total kinetic energy of the system be T_{roll} and the total potential energy of the system be V_{roll} .The dynamic equations of the longitudinal rolling subsystem are derived as:

$$\begin{bmatrix} M_{11} & M_{12} \\ M_{21} & M_{22} \end{bmatrix} \begin{bmatrix} \ddot{\alpha} \\ \ddot{\theta}_{\text{p1}} \end{bmatrix} + \begin{bmatrix} V_{11} \\ V_{21} \end{bmatrix} = \begin{bmatrix} 0 \\ \tau_{\text{p1}} \end{bmatrix} \tag{5}$$

The dynamic equations of the lateral swinging subsystem and longitudinal subsystem are the same. In practical robots, the lateral swinging subsystem is constrained by the mechanical structure of the robot, and the pendulum's range of motion is limited. The sphere cannot roll continuously, making it challenging to achieve high-dynamic motion control using the same dynamic equations. To achieve precise control of the turning radius in the spherical robot's motion, we derive the relationship between the sphere's roll angle and the turning radius is :

$$\rho = \frac{R}{tan\,(\beta)} \tag{6}$$

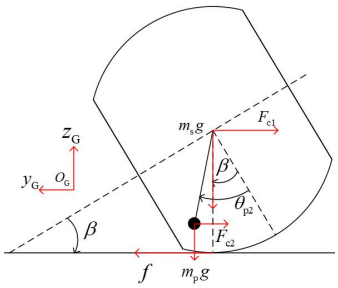

Fig. 6: Lateral rolling force analysis.

The force situation when the sphere is stably turning is shown in Figure 6. When the sphere has a longitudinal rolling velocity of $\dot{\alpha}$ and a turning radius of ρ, the centrifugal forces experienced by the sphere and the pendulum can be expressed as:

$$F_{c1} = \frac{m_s \dot{\alpha}^2 R^2}{\rho} \tag{7}$$

$$F_{c2} = \frac{m_p \dot{\alpha}^2 R^2}{\rho - L_{p2} sin(\beta + \theta_{p2})} \tag{8}$$

For this robot , $\beta + \theta_{p2}$ is small and can be considered that $\beta + \theta_{\text{p2}} \approx 0$ .The lateral friction of the sphere with the ground is:

$$f = F_{c1} + F_{c2} \approx \frac{(m_s + m_p)\dot{\alpha}^2 R^2}{\rho} \tag{9}$$

By analyzing the torque balance,combined with (6), the required pendulum angle to maintain a stable turning speed and turning radius can be expressed as:

$$\theta_{\text{p2}} = \frac{[(m_s + m_p)R - m_p L_{\text{p2}}]\dot{\alpha}^2 R^2\, tan\,\beta}{m_p g R L_{\text{p2}}} - \beta \tag{10}$$

IV. Multimodal Motion Control

A. Overall Control Framework

The software framework of the control system is illustrated in Figure 7. The Control and State Parameter Publisher publishes commands to the controller. Thread 1 is responsible for processing control and desired state parameters. Thread 2 handles the IMU data. Thread 3 has two tasks: one is to publish joint angles, speeds, and feedforward torque commands, and the other is to read the current joint state and robot's wheels information . Thread 4 is responsible for estimating the velocity of the robot's body center. Thread 5 is responsible for calculating the desired joint angles, speeds,

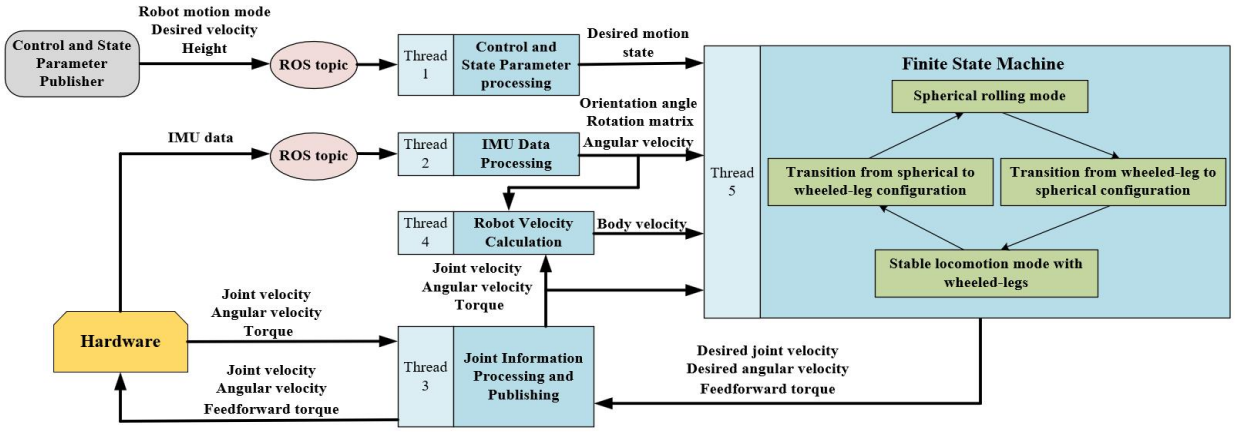

Fig. 7: System Architecture Block Diagram. Users issue commands through the upper-level interface, which are processed through ROS topics and then assigned to different threads for different tasks (blue). After receiving the commands, the robot selects the corresponding state (green), executes the tasks (yellow), and provides real-time feedback on the status through ROS topics

and torques based on the desired motion state and current state using motion control algorithms. Thread 5 utilizes finite-state machine techniques to achieve smooth transitions between various motion modes, realizing stable motion control.

B. Wheel-leg Mode Balance Control

Defining the state vector of the system under wheel-leg mode as $\boldsymbol{X} = \begin{bmatrix} \alpha & \theta_w & \theta_p & \dot{\alpha} & \dot{\theta}_w & \dot{\theta}_p \end{bmatrix}^T$. The state in which the robot's body and pendulum are both vertically aligned, and their angular velocities are zero, is the equilibrium point of the system. To simplify the design of the controller since robots typically operate near the equilibrium point, the system is linearized around the equilibrium point. (4) can be rewritten as a state-space equation:

$$\dot{\boldsymbol{X}} = \boldsymbol{A}\boldsymbol{X} + \boldsymbol{B}\boldsymbol{u} \tag{11}$$

Applying central Euler discretization to (8) yields we can get discrete linear state equation:

$$\boldsymbol{X}_{k+1} = \boldsymbol{A}_d\boldsymbol{X}_k + \boldsymbol{B}_d\boldsymbol{u}_k \tag{12}$$

To enhance the robot's resilience against external disturbances, the LQR controller is applied in this study. The quadratic performance index is defined as:

$$J = \frac{1}{2}\sum_{k=0}^{\infty}(\boldsymbol{E}_k^T\boldsymbol{Q}\boldsymbol{E}_k + \boldsymbol{u}_k^T\boldsymbol{R}\boldsymbol{u}_k) \tag{13}$$

Where $\boldsymbol{E}_k = \boldsymbol{X} - \boldsymbol{X}^{\text{des}}$ represents the state error, $\boldsymbol{X}^{\text{des}} = [0 \quad \theta_w^{\text{des}} \quad 0 \quad 0 \quad \dot{\theta}_w^{\text{des}} \quad 0]^T$ represents the desired state, and Q, R are the weight matrices , which are diagonal matrices. According to optimal control theory, it is known that this control problem has a unique optimal control input, and the optimal output is given by:

$$\boldsymbol{u}_k^* = -\boldsymbol{K}\boldsymbol{E}_k \tag{14}$$

where K is the feedback gain matrix,

$$\boldsymbol{K} = (\boldsymbol{B}_d{}^T\boldsymbol{S}\boldsymbol{B}_d + \boldsymbol{R})^{-1}\boldsymbol{B}_d{}^T\boldsymbol{S}\boldsymbol{A}_d \tag{15}$$

Matrix $\boldsymbol{S}$ is obtained by iteratively solving the discrete Riccati equation.

When operating on an incline, the equilibrium point of the robot will change . To prevent the robot's body from making contact with the slope, which can increase the risk of slippage, the robot can utilize the pendulum to adjust the center of mass position and regulate the balance pitch angle. The control function for the pendulum joint position is:

$$\theta_p^{\text{des}} = \theta_p^{\text{ref}} + (K_{\text{p,pitch}}\alpha + K_{\text{d,pitch}}\dot{\alpha})T_s \tag{16}$$

where θ_p^{des} represents the position command sent to the joint module, θ_p^{ref} is the reference position, $K_{\text{p,pitch}}$ and $K_{\text{d,pitch}}$ are the proportional and derivative coefficients, and T_s is the control period.

C. Spherical Rolling Control

In order to control the longitudinal rolling of the spherical robot,the state variables of the system are defined as follows: $e_1 = \alpha - \alpha^{\text{des}}, e_2 = \dot{\alpha} - \dot{\alpha}^{\text{des}}, e_3 = \theta_{\text{p1}} - \theta_{\text{p1}}^{\text{des}}, e_4 = \dot{\theta}_{\text{p1}} - \dot{\theta}_{\text{p1}}^{\text{des}}$. The control input is denoted as $u = \tau_p$. Assuming the external disturbances as d_1 and d_2 , by using (5), the state-space representation of the system can be obtained:

$$\begin{cases} \dot{e}_1 = e_2 \\ \dot{e}_2 = f_1 + b_1 u + d_1 \\ \dot{e}_3 = e_4 \\ \dot{e}_4 = f_2 + b_2 u + d_2 \end{cases} \tag{17}$$

The definition of the first-order sliding surface is:

$$\begin{cases} s_1 = c_1 e_1 + \dot{e}_1 \\ s_2 = c_2 e_3 + \dot{e}_3 \end{cases} \tag{18}$$

Where c_1, c_2 are sliding coefficients, and $c_1, c_2 > 0$. The first-order sliding surface is composed of two sub-sliding surfaces, corresponding to the two sets of states (e_1, e_2) and (e_3, e_4). To maintain the system's states on their respective sliding surfaces, it is necessary to satisfy $\dot{s}_1 = \dot{s}_2 = 0$. In the absence of disturbances, the equivalent control input is:

$$u_{\mathrm{eq1}} = -\frac{c_1\dot{e}_1 + f_1}{b_1}, u_{\mathrm{eq2}} = -\frac{c_2\dot{e}_2 + f_2}{b_2} \quad (19)$$

To ensure the convergence of both s_1 and s_2 to zero, a second-order sliding surface is constructed:

$$S = \lambda_1 s_1 + \lambda_2 s_2 \quad (20)$$

When the robot needs to make a turn in the spherical state, according to (10), the required pendulum angle $\theta_{\mathrm{p2}}^{\mathrm{ref}}$ to maintain a stable turning speed and turning radius can be obtained. The control equation for the roll angle during the turn is:

$$\theta_{\mathrm{p2}}^{\mathrm{des}} = \theta_{\mathrm{p2}}^{\mathrm{ref}} + K_p\left(\beta - \beta^{\mathrm{des}}\right) + K_i \int (\beta - \beta^{\mathrm{des}})dt + K_d(\dot{\beta} - \dot{\beta}^{\mathrm{des}}) \quad (21)$$

V. Prototype and Experiments

A. Prototype

The robot prototype and parameter table are shown in the Figure 10 and table 1 below.

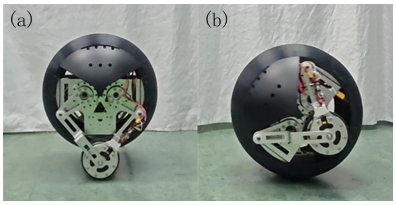

Fig. 10: The spherical wheel-legged robot. (a)In the spherical configuration . (b) In the wheel-legged configuration.

TABLE I: Technical Specifications of the robot

Category	Value
Weight	15.5kg
Minimum envelope size	40cm × 40cm × 41cm
Maximum standing height	52cm
Maximum velocity	1.1m/s

B. Experiment

(1) Impact-resistant balance

The balance experiment with impact resistance is shown as Figure 11, where a small ball weighing 2kg (12% of the robot's mass) is suspended by a rope. The ball is released at a height of 0.36m above the lowest point, causing a collision with the stationary robot at that point. The weight matrix for the LQR controller is set as $\mathrm{Q} = \mathrm{diag}(12,10,8,4,5,2)$,$\mathrm{R} = \mathrm{diag}(20,20)$, and the leg length of the robot is 0.2m. The labeled states in the Figure 11 a (1-3) represent the pre-collision, post-collision, and balanced states after recovery The pitch angle curve of the robot before and after the collision is shown in Figure 11(b). The robot takes about 1 second to regain balance during the impact, thus confirming the effectiveness of the balance control algorithm.

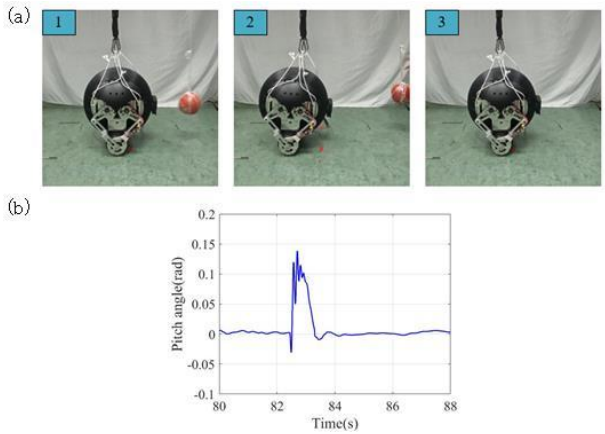

Fig. 11: Impact-resistant balance.(a) Before and after impact.(b) Pitch angle curve before and after impact.

(2) Slope climbing

In the experiment, the robot maintained stability on a 0.44 radians incline and the pitch angle curve during uphill movement as shown in Figure 12. Prior to t=96s, no center of mass adjustment was performed, resulting in a pitch angle of approximately 0.13 rad for the robot and a minimum distance of 2.7cm between the sphere shell and the inclined surface. After t=96s, center of mass adjustment was initiated, bringing the pitch angle of the robot close to 0 rad and increasing the minimum distance between the sphere shell and the inclined surface to 4.2cm.

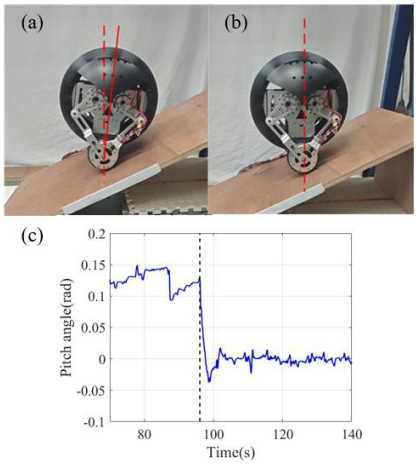

Fig. 12:Slope climbing.(a) No mass adjustment.(b) Mass adjustment (c) Slope pitch angle

(3) Roll angle stabilizing

Figure 13 represents the experiment on roll angle stability. The PID control parameters used were $\mathrm{K_p} = 8.2, \mathrm{K_i} = 0.05, \mathrm{K_d} = 2.0$. In the experiment, the robot was pushed from the side to a certain angle and then the applied force was removed. The robot's roll angle quickly recovered while suppressing oscillations, eventually converging to 0 rad. The experiment involved pushing the robot a total of three times. The roll angle curve is shown in Figure 13, confirming the

effectiveness of the PID algorithm in stabilizing the roll angle of the sphere.

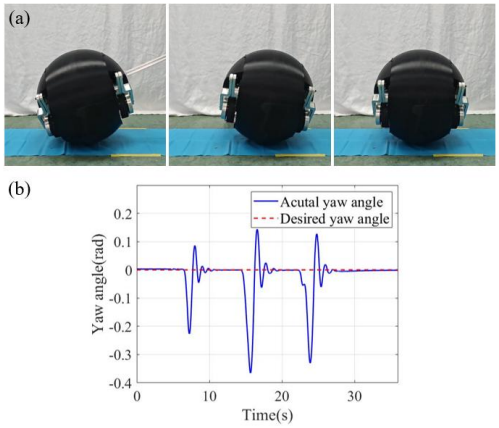

Fig. 13:Roll angle stabilizing.(a) Roll angle stability experiment.(b) Roll angle curve under disturbance.

(4) Longitudinal rolling

Figure 14 depicts the experiment on longitudinal roll angle control and the roll angle curve. The parameters of the hierarchical sliding mode controller used were $c_1 = 0.25, c_2 = 5.5, \lambda_1 = 3, \lambda_2 = 1, k = 7.5, \eta = 23.5$. In the experiment, the robot was able to quickly roll to the desired angle with minimal oscillations commonly observed in spherical robots. The convergence time was approximately 2 seconds, and the maximum steady-state error occurred during the second roll, measuring only 0.07 radians, corresponding to a relative error of 1.1%. These results validate the proposed roll control method in this study, which demonstrates high stability, fast response, and low steady-state error characteristics.

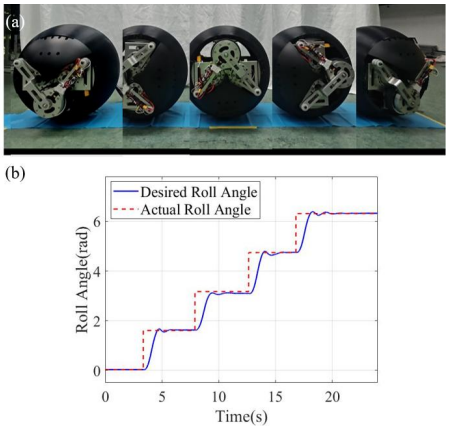

Fig. 14:Longitudinal rolling. (a) Longitudinal roll angle control experiment (b)Roll angle curve during longitudinal rolling.

VI. CONCLUSIONS

The paper presents a spherical wheeled-leg mobile robot and establishes the dynamic equations for the robot's leg motion mode and spherical rolling mode based on the designed mechanical structure. In the balance control section, a pendulum-wheel inverted pendulum dynamic model is established, and the optimal control torque is calculated based on this model combined with the LQR controller. In the rolling control section, a hierarchical sliding mode control and PID balance control method are proposed to achieve steering control. The proposed control strategies are validated through simulations and experiments on a prototype. In the wheel-legged mode, the robot can achieve a maximum speed of 1.1 m/s and maintain a stable climbing on a 0.44 radians slope with a pitch angle around 0 rad, effectively avoiding contact with the sphere and the slope. In the longitudinal rolling experiment, the robot converges to a stable angle within 2 seconds, with a maximum steady-state error of 0.07 radians and a relative error of 1.1%, demonstrating good stability and fast response speed.

REFERENCES

[1] Bicchi A, Balluchi A, Prattichizzo D, et al. Introducing The "SPHERICLE": An Experimental Testbed for Research and Teaching in Nonholonomy[C]//Proceedings of IEEE International Conference on Robotics and Automation (ICRA). Albuquerque, New Mexico, 2002:2620-2625.

[2] Sun H, Xiao A, Jia Q, et al. Omnidirectional Kinematics Analysis on Bi-Driver Spherical Robot[J]. Journal of Beijing University of Aeronautics and Astronautics, 2005, 31(7):735-739.

[3] Kaznov V, Seeman M. Outdoor Navigation with A Spherical Amphibious Robot [C]//Proceedings of IEEE/RSJ International Conference on Intelligent Robots and Systems (IROS). Taipei, Taiwan, 2010:5113-5118.

[4] Zhan Q, Cai Y, Yan C. Design, Analysis and Experiments of an Omni-Directional Spherical Robot[C]//Proceedings of IEEE International Conference on Robotics and Automation (ICRA). Shanghai, China, 2011:4921-4926.

[5] Kim Y, Ahn S, Lee Y. KisBot: New Spherical Robot with Arms[C]//Proceedings of the WSEAS International Conference on Robotics, Control and Manufacturing Technology. Wisconsin, USA, 2010:63-67.

[6] Sun H, Zhao W, Zhang Y. Mechanical Analysis about A New Kind of Variable Structure Spherical Mobile Robot[J]. Journal of Mechanical Engineering, 2013, 49(19):40-47.

[7] Raura L, Warren A, Thangavelautham J. Spherical Planetary Robot for Rugged Terrain Traversal[C]//Proceedings of IEEE Aerospace Conference. Yellowstone Conference Center, USA, 2017:1-10.

[8] Chang W, Chang C, Ho J, et al. Design and Implementation of a Novel Spherical Robot with Rolling and Leaping Capability[J]. Mechanism and Machine Theory, 2022, 171:10474.

[9] Kinjo T, Aoki T. Development of Quadruped Walking Robot with Spherical Shell: Improvement of Climbing over A Step[J]. ROBOMECH Journal, 2017, 7(22):1-12.

[10] Xu L, Zhou H, Feng H, et al. Design and Experiments of a Novel Hydraulic Wheel-Legged Robot (WLR)[C]//Proceedings of the IEEE/RSJ International Conference on Intelligent Robots and Systems (IROS). Madrid, Spain, 2018:3292-3297.

[11] Li X, Zhou H, Zhang S, et al. WLR-II: A Hose-less Hydraulic Wheel-legged Robot[C]//Proceedings of the IEEE/RSJ International Conference on Intelligent Robots and Systems (IROS). Macau, China, 2019:4339-4346.

[12] Klemm V, Morra A, Salzmann C, et al. Ascento: A Two-Wheeled Jumping Robot[C]//Proceedings of IEEE International Conference on Robotics and Automation (ICRA), Montreal, Canada, 2019:7515-7521.

[13] Wang S, Cui L, Zhang J, et al. Balance Control of a Novel Wheel-Legged Robot: Design and experiments[C]//Proceedings of IEEE International Conference on Robotics and Automation (ICRA). Xi'an, China, 2021:6782-6788.